Calculations on the slowing down of 0.4–4.0-MeV He ions in solids*

B. M. Latta and P. J. Scanlon
Queen's University, Kingston, Ontario, Canada K7L 3N6
(Received 27 February 1975)

The localization of atoms in solids leads, in principle, to changes in the electron distribution compared with the free-atom state. The effect of such changes on the calculation of the He-ion stopping cross section S_e in solids has been investigated for an energy range 0.4–4.0 MeV. It is found that at low energies with free-atom wave functions, a large part of the calculated S_e arises from regions at large distances from the target atom where the electron density is low compared to that in solids. The experimentally observed oscillations in S_e as a function of target atomic number, which have been calculated from stopping-power theory by other authors, are also obtained in the present work with simple modifications of the electron density distributions. However, the detail of the structure of the stopping curves is altered. In addition, the use of an effective charge to account for electron capture by the He ion at low velocities, without a corresponding modification of the basic stopping-power theory to take into account the departure from point-charge behavior, leads to discrepancies from the experimental data.

I. INTRODUCTION

The increasing use of accelerated helium beams as probes for investigating solids plus improvements in experimental techniques have led to a need for accurate estimates of their stopping powers in matter. For experimental reasons the investigations are conducted at moderately high beam velocities. At these velocities the energy loss is mainly electronic and is due to the projectile's interaction with the electrons of the solid. The nuclear energy loss component arising from the target-atom recoil is usually included only if backscattering occurs and then only at the particular collision causing backscattering of the beam.

The theoretical problem of electronic stopping powers has been approached from the two limits of high and low velocity. Low here refers to velocities at which the projectile is neutral, while high refers to velocities for fully stripped projectiles.

At low velocity the electronic energy loss has been treated by Firsov[1] as being due to the exchange of electrons between projectile and target. The electrons picked up by the projectile must be accelerated to the projectile's velocity, and thus the flux of electrons from target to projectile produces a drag force on the projectile. Modifications by several authors[2–5] to include atomic shell structure have led to explanations for the experimentally observed Z_1 and Z_2 oscillations in stopping cross sections at low velocities (Z_1 refers to the projectile, Z_2 to the target).

At high velocities the projectile picks up few, if any, electrons and the main interaction is through the electric field of the unscreened nucleus as it sweeps past the target electrons. This mechanism for energy loss as formulated by Lindhard-Scharff-Winther[6–8] (LSW) has been used by Ziegler and Chu[9] to calculate the rate of energy loss of $^4He^{++}$ ions moving through gases and solids. Their calculations reproduce the general oscillatory behavior of the experimental results, but vary somewhat in detailed structure from experiment. A semiempirical fitting procedure was adopted by them to scale their theoretical results in regions where no experimental data existed.

In the following sections we investigate the LSW theory as it applies to the velocity region spanned by the tabulation of Ziegler and Chu.

II. LINDHARD-SCHARFF-WINTHER THEORY

Using the random-phase-approximation result for the dielectric constant of a uniform electron gas, Lindhard has derived expressions for the electronic energy loss.[6] The rate of energy loss is given by

$$\frac{dE}{dx} = -\frac{4\pi Z_1^2 e^4}{m v^2} n L(n, v), \tag{1}$$

where v is the velocity of the projectile relative to the electrons, m the electron mass, n the electron density, and L is a dimensionless quantity.

Lindhard and Scharff[7] have extended this theory to an electron gas in which there is a distribution of densities by carrying out an average over the possible electron densities present. If there are N atoms per unit volume, each with a radially symmetric charge density $\rho(r)$, then the probability of finding the electron density $\rho(r)$ is proportional to $N4\pi r^2\, dr$ and the resulting stopping cross section is

$$S_e = -\frac{1}{N}\frac{dE}{dx} = \frac{4\pi Z_1^2 e^4}{mv^2}\int_0^\infty \rho(r) L(\rho(r), v) 4\pi r^2 dr, \tag{2}$$

where $\rho(r)$ is normalized to the charge of the target atom by

$$\int_0^\infty \rho(r) 4\pi r^2 dr = Z_2 . \tag{3}$$

Lindhard and Winther[8] have studied asymptotic forms of $L(\rho, v)$ whose domains of validity are defined with respect to the electron Fermi velocity (v_F) in the target, where

$$\tfrac{1}{2} m v_F^2 = (\hbar^2/2m)(3\pi^2\rho)^{2/3} . \tag{4}$$

The expressions for L are then (Ref. 8)

$$L(\rho, v) = \begin{cases} C_1(\chi)(v/v_F)^3, & v \leq v_F \\ \ln(y) - 3^{3/2}/(5\chi y) - 9/(14\chi^2 y^2)\cdots, & v \geq v_F \end{cases} \tag{5}$$

$$C_1(\chi) = \frac{1}{2(1-\chi^2/3)^2}\left[\ln\left(\frac{1+\frac{2}{3}\chi^2}{\chi^2}\right) - \frac{1-\frac{1}{3}\chi^2}{1+\frac{2}{3}\chi^2}\right],$$

$$\chi^2 = e^2/\pi\hbar v_F, \qquad \chi y = \sqrt{3}(v/v_F)^2 .$$

The expression for $C_1(\chi)$ in Ref. 8 has an incorrect sign (see Ref. 9). There are also missing powers in Eq. A5 and the succeeding definition of y in Ref. 9.

For $v \gg v_F$ the LSW result approaches the Bethe-Bloch form, while for $v \leq v_F$ the stopping becomes proportional to the velocity.

The expressions for L are approximations and are generally not continuous at $v = v_F$. In our calculations below, the branch point for the calculation of $L(\rho, v)$ from Eq. (5) was determined from the matching point of the two solutions to avoid a finite discontinuity in L. The branching value of $v_F(r)$ was always close to v.

The free-electron-gas model may be applied to bound electrons as long as $\chi^2 < 1$.[8] This condition is satisfied for the densities of electrons found in solids.

III. CALCULATIONS

A. Target-atom size

Ziegler and Chu[9] use Hartree-Fock-Slater (HFS) wave functions for a free atom for the electron density in their calculations. Since most targets exist in the solid state and thus the exact free-atom wave functions are not strictly correct, a less powerful free-atom solution is sufficient for investigative purposes. We have repeated the Ziegler and Chu calculations using Slate-type-orbital (STO) fits to the HFS total density as tabulated by Clementi.[10,11] Figure 1 shows the ratio of the stopping powers calculated from the Clementi STO's to the stopping powers tabulated by Ziegler and Chu. The comparison is made at 400 and 4000 keV, corresponding to the low and high energy range of their tabulation. The deviations at the gases around Ne are of no interest to the present discussion as we restrict our further analysis to solid target materials. We also delete

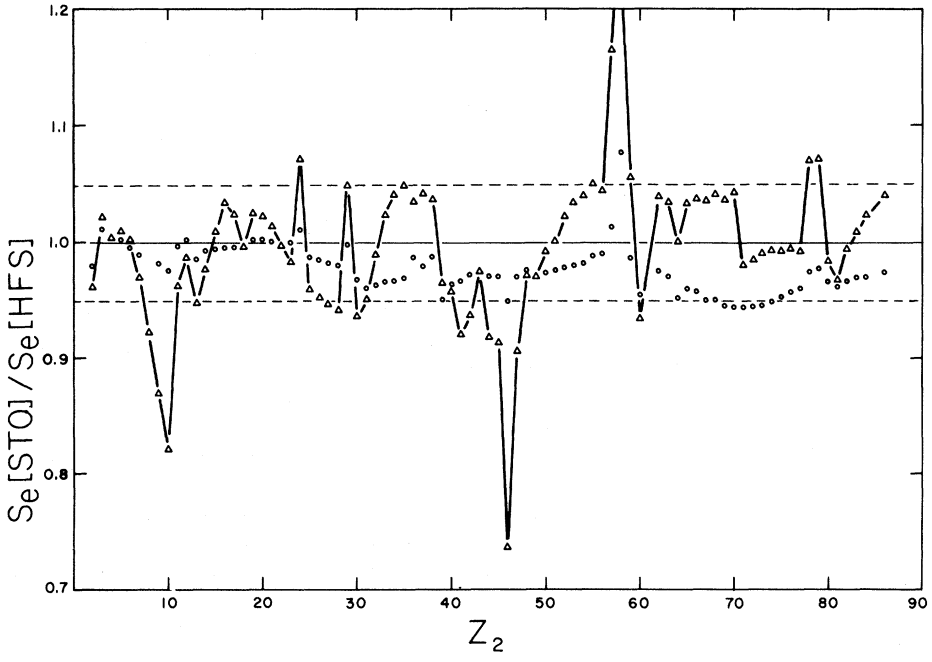

FIG. 1. Comparison of the ^{4}He electronic stopping cross sections evaluated using free-atom Slater-type orbitals (STO) with those tabulated by Ziegler and Chu based on free-atom Hartree-Fock-Slater (HFS) wave functions as a function of target atomic number Z_2. The triangles and open circles correspond to 0.4 and 4.0 MeV, respectively.

the targets with Z values of 46, 57, and 58. Clementi[11] has cautioned that he had difficulty in obtaining a good fit for Z values from 57 to 60. The origin of the discrepancy at $Z=46$ is not clear. For all the remaining targets the Ziegler and Chu results are reproduced with the simpler STO's to within 10%, while for most targets the calculations agree within 5%.

The HFS free-atom wave functions do not satisfy the correct boundary conditions for a solid target. In a solid the target atom occupies some finite volume inside of which there will be Z_2 electrons on the average. Thus the electron density attributed to each atom should not be distributed over an infinite region. The significance of this fact can be seen by considering the size of the contribution to the integral in Eq. (2) from regions inside and outside of a distance r_0, where r_0 is a size parameter given by

$$r_0=(\tfrac{4}{3}\pi N)^{-1/3}\sim\frac{1}{1.612}N^{-1/3} \tag{6}$$

and is of the order of half the interatomic spacing in a solid. The value of N can be determined from the bulk density. The fraction

$$F(Z_2,r_0)=\frac{\int_0^{r_0}\rho(r)L(\rho,v)r^2\,dr}{\int_0^{\infty}\rho(r)L(\rho,v)r^2\,dr}$$

is shown in Fig. 2 for helium at 400, 1000, and 4000 keV. For a 400-keV helium beam the fraction of the integration lying inside of r_0 may be as low as 50% and is less than 70% for most targets. Therefore, generally more than 30% of the integral is calculated in a region where the density is not given correctly by the free-atom wave functions. The small amount of charge outside of r_0 contributes significantly to the stopping cross-section calculations and is of increasing importance as the projectile velocity decreases. Hence some modification of the charge density used to obtain the stopping cross sections in solids is necessary.

Assuming that the basic structure in the HFS solutions for $\rho(r)$ will be modified in the region $r\sim r_0$, we have renormalized the density by

$$\int_0^{r_0}\rho'(r)4\pi r^2\,dr=Z_2$$

with

$$\rho'(r)=\rho(r)+Cr^p \tag{7}$$

where $\rho(r)$ is the Clementi fit to the HFS density, the power p can be set arbitrarily, and C is a normalization constant. The form Cr^p for the additional term in the density gives a simple method of obtaining different distributions, over the region bounded by r_0, for the charge originally outside of r_0. For $p=0$ the additional charge is spread uniformly over the spherical volume; for $p=2$ it is more concentrated at the surface of the sphere of radius r_0. When $\rho'(r)$ from Eq. (7) replaces $\rho(r)$ in Eq. (2) the upper limit on the integration becomes r_0.

The integrand of Eq. (2) for a Au target is shown in Fig. 3 for different electron density distributions and two beam energies. The discontinuity in the

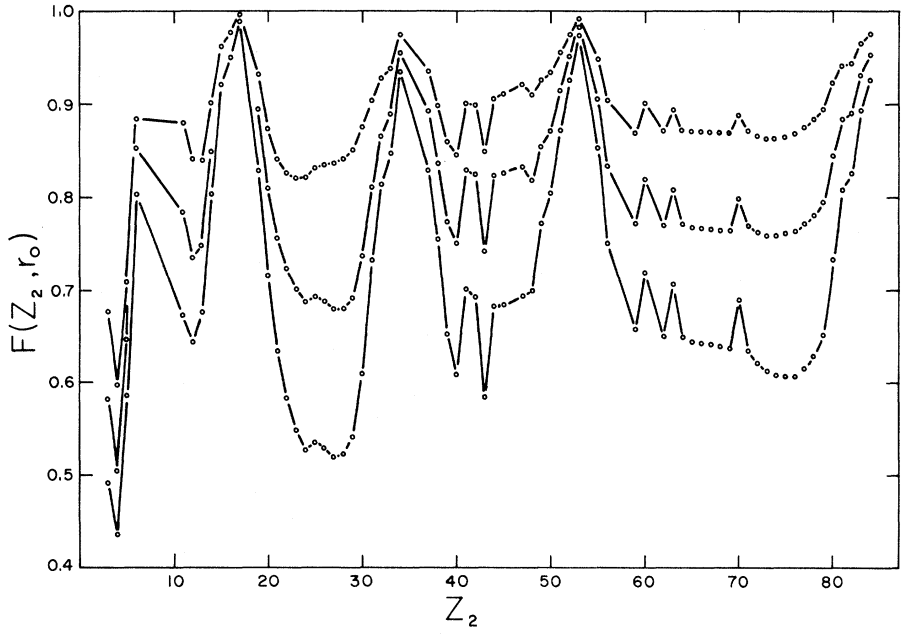

FIG. 2. Fraction of the ^{4}He electronic stopping cross-section calculation occurring inside of an atomic size parameter $r_0=0.62N^{-1/3}$ versus target atomic number Z_2. The upper, middle, and lower curves correspond to calculations for ^{4}He energies of 4.0, 1.0, and 0.4 Mev, respectively.

slope at about 1.1 and 1.6 Bohr radii for the 1000 and 400 keV curves occurs at the matching point of the asymptotic solutions to L. This feature is less pronounced at higher energies. As the energy increases, the peak position continues to shift toward the origin. For the two energies shown, 17.5% and 35%, respectively, of the integral fall outside of r_0 when a free-atom electron density is employed. Also plotted are curves based on the renormalized density with $p=0$ and 2 in Eq. (7). The final integral is not very sensitive to the choice of p in the renormalization procedure. However, any Z_2 fine structure in the free-atom stopping cross sections that results from the density variations at $r \gtrsim r_0$ has been eliminated in the calculation for a solid. In addition the density near r_0 is modified, altering the effect of structure in the original free-atom density. These modifications will be most important at low energies.

Figure 4 shows the stopping cross section as a function of target atomic number. The upper and lower curves are calculated for a free-atom electron density (the lower one giving the contribution only out to r_0). The middle curve joins points obtained when a Cr^2 term is used to renormalize the density. There is some modification of the fine structure, but the main oscillations are still present. The differences between the curves is not as apparent in regions of steep ascent such as at $^{27}_{13}$Al where the curves have values of 63, 81.5, and 98.6 eV cm^2/10^{15} atoms.

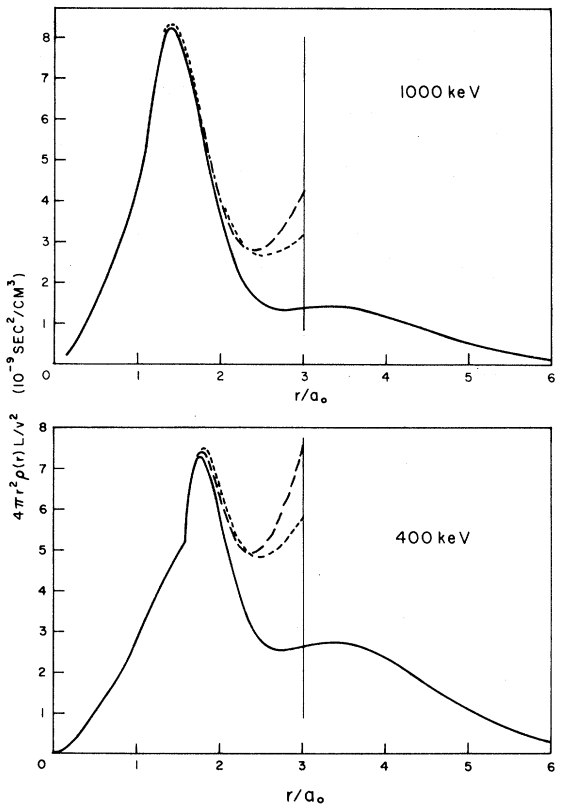

FIG. 3. Integrands for the ^{4}He stopping cross section in gold, at two ^{4}He projectile energies, for different assumed target electron densities. The solid curves are for free-atom distributions ρ. The dashed curves are for densities renormalized by $\int_0^{r_0} 4\pi r^2(\rho + C)\,dr = Z_2$, and the broken curves are for densities renormalized by $\int_0^{r_0} 4\pi r^2(\rho + Cr^2)\,dr = Z_2$, where $r_0 \approx 3a_0$ for gold.

B. Projectile charge state

In the calculations thus far we have assumed (as Ziegler and Chu[9]) that the helium projectile is doubly charged. If the helium ion is not fully stripped the stopping cross-section calculation in Eq. (2) must be modified.

The LSW calculation for the stopping cross section S_e is based on the assumptions (a) that a point charge Z_1 is moving in a dielectric medium and (b) that S_e can be expressed in terms of a product of the charge squared and a function L that depends only on the electron density of the stopping material and the velocity of the projectile relative to the electrons. If the moving ion picks up electrons, then for distances greater than the dimensions of the moving charge distribution it will appear, at least to a first approximation, as a point charge with an effective charge $\gamma Z_1 e$. The effec-

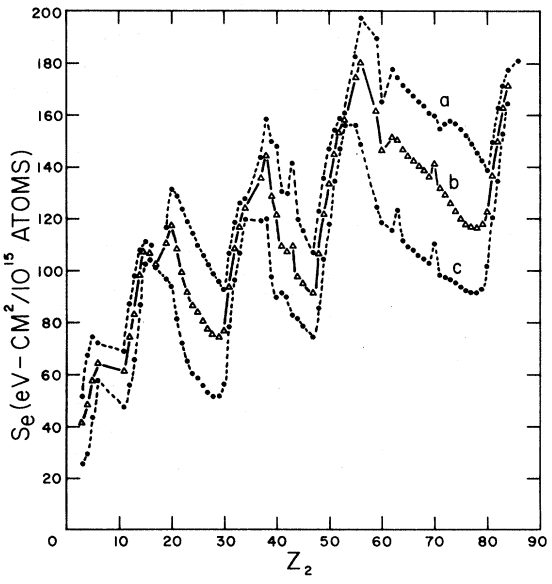

FIG. 4. Theoretical stopping cross sections for 400-keV ^{4}He as a function of target atomic number Z_2. (a) for free-atom electron densities $\rho(r)$, (b) for electron densities renormalized by $\int_0^{r_0} 4\pi r^2(\rho + Cr^2)\,dr = Z_2$, (c) for free-atom electron densities with the calculation truncated at $r = r_0$.

tive charge is obtained from (see the review paper by L. C. Northcliffe[12])

$$(\gamma Z_1)^2 = \sum_{i=1}^{Z} i^2 \phi_i , \quad \sum_{i=0}^{Z} \phi_i = 1 , \tag{8}$$

where i is the charge state and ϕ_i is the population of that state.

If the major part of the calculation for L comes from regions outside of the radius of the projectile charge distribution, then S_e can be determined as for a point charge of value $\gamma Z_1 e$. However, according to Bohr and Lindhard[13] the finite extent of the moving charge distribution is important for high-Z_1 projectiles at low velocities, such as fission fragments, since colliding electrons that penetrate the moving electron distribution are affected by a higher net charge than $\gamma Z_1 e$. Basically this effect results in a greater value of S_e than would be obtained for the corresponding effective point charge. The calculation of $L(\rho, v)$ for low velocities must be replaced by $L(\rho, v, \gamma Z_1)$ which includes the dependence on the projectile charge distribution.

At sufficiently low velocities of the He projectile a major portion of the calculation of L comes from impact parameters that correspond to paths inside of a He atom electron distribution. As an example we consider 400-keV helium. At nonrelativistic speeds there is negligible energy loss to electrons whose impact parameter with respect to the projectile is greater than $b_{max} \sim v/\omega$, where $\omega = (4\pi e^2 \rho/m)^{1/2}$ is the plasma frequency for a gas of electron density ρ.[6,14] Each target atom has a range of electron densities $\rho(r)$. On averaging over the electron charge distribution to obtain the mean stopping cross section in Eq. (2), a maximum in the integrand occurs at some specific electron density. As may be seen in Fig. 3 this maximum occurs at about two Bohr radii or a density $\rho(2a_0)$ for the Au target electron distribution. Using this density for a renormalized STO, we obtain a b_{max} of approximately 1 Å. The b_{max} in carbon at a density of $\rho(2a_0)$ for the renormalized STO is only slightly larger at 1.6 Å. Since this is of the same order as the size of an atom, the calculation will be modified if the helium projectile carries any electrons at this energy.

Using the charge state values from Table VI-15 of S. K. Allison[15] in Eq. (8), we have calculated the effective charge for helium. This is plotted in Fig. 5. Clearly, below 2 MeV it is important to take the effective charge into account. At 400 keV, 15% of the beam is neutral while 65% is singly charged.

One further investigation can be made without an explicit calculation of the more appropriate $L(\rho, v, \gamma Z_1)$. If point charges of $Z_1 e$ and $\gamma Z_1 e$ are used with $L(\rho, v)$ in Eq. (2), we should obtain upper and lower bounds, respectively, on the stopping cross section. Figure 6 shows the values obtained for S_e based on the renormalized electron density from Eq. (7) with $p = 2$. At a helium beam energy of 400 keV the curves do indeed bound the experimental measurements with only a few exceptions. Since, as discussed earlier, the main energy loss at this velocity is to electrons that penetrate the ion's electron distribution, most electrons see an effective point charge greater than would be experimentally measured. It would appear from Fig. 6 that in many targets one would be more in error using an experimental $\gamma Z_1 e$ with the unmodified L calculation than one would be by using $Z_1 e$ for the point charge. At 1000 keV almost all of the experimental measurements lie above the calculated upper bound. The simple inclusion of an effective point charge only increases the discrepancy.

IV. SUMMARY

The experimental Z_2 oscillations in the He stopping cross sections have been reproduced using both the simpler STO's for free atoms and renormalized STO's for atoms in solids. The fine structure on these oscillations is modified when a renormalized density for a solid is employed. Ziegler and Chu[9] have adopted a semiempirical approach where the stopping cross section is scaled to the existing experimental data. Differences in the fine structure that are associated with the choice of the wave function will lead to errors in the interpolated values. In addition, at low energies this semiempirical procedure may lead to

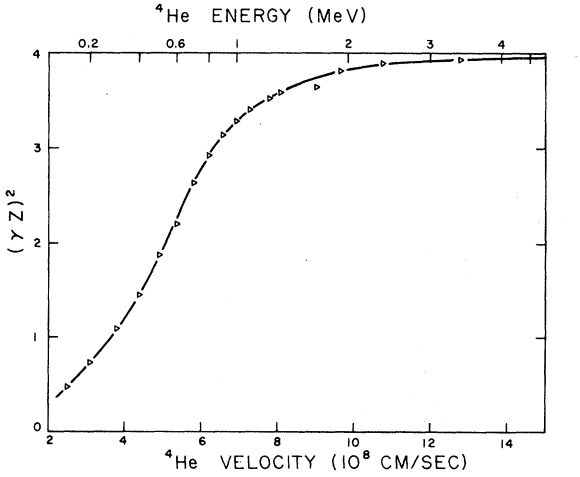

FIG. 5. Square of the effective charge of ^{4}He projectiles (in units of e^2). The open triangles are calculated from the experimental charge fractions in Ref. 15. The solid curve is drawn through the points to show the trend of the data.

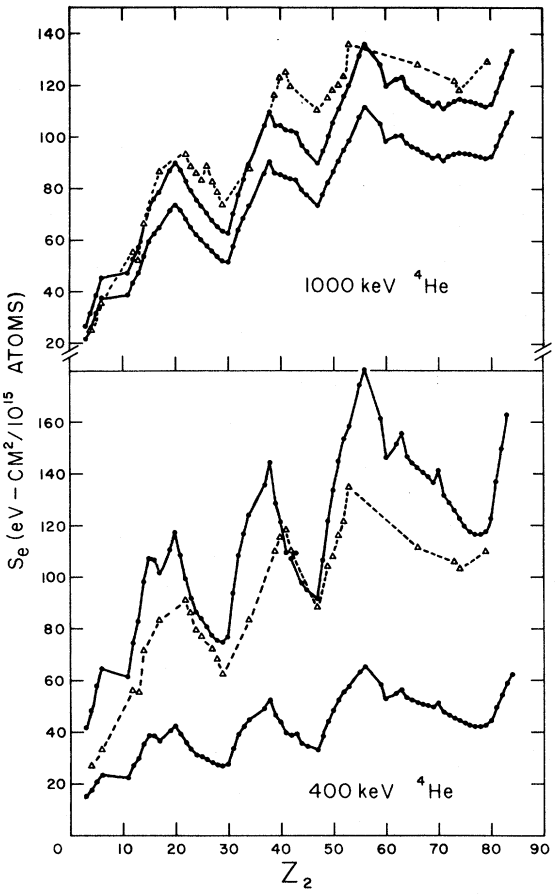

FIG. 6. Comparison of the estimated upper and lower bounds (solid curves) of the stopping cross sections of ^{4}He according to the Lindhard-Scharff-Winther theory. The triangles represent experimental results taken from Ref. 9.

erroneous results since a modified treatment of L, due to the nonpoint nature of the projectile charge distribution, could change the oscillatory structure. The inclusion of screening of the He ion through the use of an effective point charge as by Northcliffe[12] without a corresponding change in $L(\rho, v)$ leads to values of S_e that are generally too low.

Although the oscillations at a helium beam energy of 1000 keV were reproduced in the present calculations, the magnitude of the expected upper bound was somewhat low. This may be the result of one of several approximations: (a) The electron charge distributions used for the solids are only approximate, both because of the *ad hoc* form of the renormalization and because no solid-state structure effects are included. It should be noted that the recent tables of Clementi and Roetti,[16] which supersede the ones used in this work, are still fits to the free-atom HFS wave functions. Since the LSW theory uses the total electron density the structure of the individual orbits is not critical. The earlier tabulation, which gives results for stopping powers close to those based on HFS wave functions (Fig. 1), is adequate for the calculations presented in this paper. (b) The solutions for L appropriate for a free gas are only for a first-order linear treatment of the equations. The form of L given by Eq. (5) is itself an approximation to this solution. (c) Since the polarization of an electron gas at any point depends on the electron density occurring nearer to the projectile, the extension of the solution for a uniform gas by an average over the target-atom density distribution in Eq. (2) may introduce some error.

As a result of the above considerations it is clear that for accurate theoretical estimates of the stopping cross section, more reliable estimates of the electron densities in solids are required together with a knowledge of the dependence of L on the charge state of the projectile.

*Work supported by the Atomic Energy Control Board of Canada.

[1]O. B. Firsov, Zh. Eksp. Theor. Fiz. 36, 1517 (1959) [Sov. Phys.—JETP 9, 1076 (1959)].
[2]K. B. Winterbon, Can. J. Phys. 46, 2429 (1968).
[3]I. M. Cheshire, G. Dearnaley, and J. M. Poate, Phys. Lett. 27A, 304 (1968).
[4]C. P. Bhalla, J. N. Bradford, and G. Reese, *Atomic Collision Phenomena in Solids*, edited by D. W. Palmer, M. W. Thompson, and P. D. Townsend (North-Holland, Amsterdam, 1970), p. 361.
[5]F. F. Komarov and M. A. Kumakhov, Phys. Stat. Sol. B 58, 389 (1973).
[6]J. Lindhard, K. Dan. Vidensk. Selsk. Mat.-Fys. Medd. 28, No. 8 (1954).
[7]J. Lindhard and M. Scharff, K. Dan. Vidensk. Selsk. Mat.-Fys. Medd. 27, No. 15 (1953).
[8]J. Lindhard and A. Winther, K. Dan. Vidensk. Selsk. Mat.-Fys. Medd. 34, No. 4 (1964).
[9]J. F. Ziegler and W. K. Chu, At. Data Nucl. Data Tables 13, 463 (1974).
[10]E. Clementi and D. L. Raimondi, J. Chem. Phys. 38, 2686 (1963).
[11]E. Clementi, D. L. Raimondi, and W. P. Reinhardt, J. Chem. Phys. 47, 1300 (1967).
[12]L. C. Northcliffe, Ann. Rev. Nucl. Sci. 13, 67 (1963).
[13]N. Bohr and J. Lindhard, K. Dan. Vidensk. Selsk. Mat.-Fys. Medd. 28, No. 7 (1954).
[14]J. D. Jackson, *Classical Electrodynamics* (Wiley, New York, 1962), p. 432.
[15]S. K. Allison, Rev. Mod. Phys. 30, 1137 (1958).
[16]E. Clementi and C. Roetti, At. Data Nucl. Data Tables 14, 177 (1974).